

## Research Article

### A Novel Control Method for BLDCM Based on Phase Back-EMF Observation

<sup>1,2</sup>Pan Lei, <sup>2</sup>Wang Bei-Bei and <sup>1</sup>Sun He-Xu

<sup>1</sup>Control Science and Engineering School, Hebei University of Technology, Tianjin, China

<sup>2</sup>Department of Electronic and Information Engineering, Tianjin Institute of Urban Construction, Tianjin, China

**Abstract:** The main purpose of this study is to propose a novel back-EMF observer. It can drive a permanent magnet Brushless DC Motor (BLDCM) smoothly from slow to high speed without position or speed sensors. In the method, a phase back-EMF observer, which could estimate phase back-EMFs in real time and only relies on DC voltage and phase currents of motor without an additional circuit or complicated operation process, had been established with phase back-EMF as a disturbance signal. This observer simplifies the structure of traditional back-EMF observers and only has one inertia element, hence the response time and robustness of the system could be improved. This study also detailedly provides a method for speed and position detection, which has high performance in low speed range. The validity of the proposed method is verified through simulation and experimental results.

**Keywords:** BLDCM, phase back-EMF observer, position-sensorless control, whole speed range

## INTRODUCTION

BLDCM is widely used in various applications of electromechanical systems because of its high efficiency, high power density and good controllability over a wide range of speed and low maintenance cost due to the removal of the brushes (Wang *et al.*, 2010; Bharatkar and Yanamshetti, 2010; Wang and Liu, 2008).

A BLDCM requires an inverter and a rotor position sensor to perform commutation process. However, the position sensor presents several disadvantages in view of drive's cost, machine size, reliability and noise immunity. As a result, many sensorless drive solutions have been developed to eliminate the costly and fragile position sensor for BLDCM with trapezoidal back-EMFs. Therefore, several main techniques of sensorless control of BLDCM have been extensively studied and can be categorized as followed:

Firstly, Stator Inductance Method (Yen-Shin, 2004; Xianxiang *et al.*, 2009) is proven to be independent of rotor velocity in the whole speed range and be successful to detect rotor position at very low speed. But the inverter loss and the torque ripple in BLDCM are very serious, for H\_PWM-L\_PWM modulation is used in indirect inductance method. In order to overcome these shortcomings, it is necessary to combine this method with other control methods to realize the high-efficiency operation without position sensor at both low speed and high speed.

Secondly, observer Method (Changliang *et al.*, 2006; Kim and Sul, 1995; Furuhashi *et al.*, 1990; Guan *et al.*, 2005) can be used to real-timely estimate the rotor position and speed by sliding mode observer, Luenberger observer, fuzzy logic-based neural network observer or other state observers. In this method a detailed motor mathematical model is required. In addition, phase voltages have to be measured and A/D converters are required. In order to reduce the number of voltage transducers, voltages can be deduced from the inverter switching status and the measured dc-link voltage. But torque ripple, inaccuracy of angle and speed estimation at low speed and algorithm complexity are main problems.

Thirdly, detecting method of freewheeling diode (Tae-Sung, 2008; Ungurean *et al.*, 2010) is a technique for detection of the conducting state of freewheeling diode in unexcited phase. It has simple synchronous process and perfect control characteristic at low speed. However, detecting precision of rotor position conspicuously degrades at high speed. In particular, additional isolated power has been needed to supply to a comparator for detecting the freewheeling current in this method.

Fourthly, Back-EMF Sensing Techniques include detection of the zero crossing of back-EMF (Zicheng *et al.*, 2009) and back-EMF-based sensorless techniques (Ungurean *et al.*, 2010; Zicheng *et al.*, 2009). Methods based on detection of the zero crossing of back-EMF are simple and various commercial ICs are available for

**Corresponding Author:** Pan Lei, Department of Electronic and Information Engineering, Tianjin Institute of Urban Construction, Tianjin, China. Tel.: 13512241509

This work is licensed under a Creative Commons Attribution 4.0 International License (URL: <http://creativecommons.org/licenses/by/4.0/>).

BLDCM drive. However, they could not be applied to BLDCM operation if the commutation advance or the current decay in the freewheeling diodes is greater than 30 electrical angles, since the zero crossing of back-EMF cannot then be detected. In back-EMF-based sensorless techniques, most of the low-speed performance is limited. But the problem had been solved (Tae-Sung, 2008), in which a line-to-line back-EMF observer is established through regarding line-to-line back-EMF as unknown input. It could realize the whole speed range control of BLDCM without using position sensor. However, there are two first-order inertia elements, which lead to prolonging of transition process and increasing pulsation of rotor speed and torque. In addition, a method of back-EMF sliding-mode observer for BLDCM which is exploiting the mathematical relationship between the speed and the back-EMF is proposed (H.Fakham *et al.*, 2008). A novel Variable Structure Control scheme of BLDCM is proposed (Changliang *et al.*, 2005), in which current fluctuation caused by current commutating is treated as a disturbance. Based on the above results, this study is proposed.

This study proposes a novel sensorless control method. In the method, a phase back-EMF observer, which could estimate phase back-EMFs in real time and only relies on DC voltage and phases current of motor without an additional circuit or complicated operation process, had been established with phase back-EMF as a disturbance signal. This observer simplifies the structure of traditional back-EMF observers and only has one inertia element, hence the response time and robustness of the system could be improved. In addition, this method shows the basic structural relationship between the change of phase current and phase back-EMF and provides reference for using other methods (such as PID, self-adaptive or artificial intelligence control) to realize phase back-EMF estimation. This study proposes a detection method of speed and position detailedly and the method has high performance at low speed range. The results of simulations and experiments show the validity of this algorithm for BLDCM control.

### MODELLING OF BLDCM

The ordinary BLDCM applies three-phase VSI (voltage source inverter) for power supply and its stator winding is connected in star. Because the neutral point of BLDCM is not extracted, the phase voltage equation is difficult to be accurately constructed. The line-to-line voltage expressions could be obtained through corresponding subtraction of the three-phase phase voltages (Shao, 2006):

$$\begin{cases} u_{ab} = R_s(i_a - i_b) + Lp(i_a - i_b) + (e_a - e_b) \\ u_{bc} = R_s(i_b - i_c) + Lp(i_b - i_c) + (e_b - e_c) \\ u_{ca} = R_s(i_c - i_a) + Lp(i_c - i_a) + (e_c - e_a) \end{cases} \quad (1)$$

where,

- $p$  = Differential operator  $d/dt$
- $R_s$  = Stator resistance
- $L_s$  = Self-inductance of stator winding
- $M$  = Mutual inductance of stator winding and  $L = L_s - M$
- $i_a, i_b, i_c$  = Phase currents
- $e_a, e_b, e_c$  = Phase back-EMFs

Further consider the difference between line-voltages and the following equation could be obtained after subtracting  $u_{bc}$  from  $u_{ab}$ :

$$u_{ab} - u_{bc} = R_s(i_a + i_c - 2i_b) + Lp(i_a + i_c - 2i_b) + (e_a + e_c - 2e_b) \quad (2)$$

Supposing that phase A and phase C are conducted and phase B is not conducted, then  $e_a + e_c = 0$ . Because three stator windings of BLDCM are connected in star,  $i_a + i_b + i_c = 0$  and (2) could be simplified as:

$$u_{ab} - u_{bc} = -3R_s i_b - 3Lp i_b - 2e_b \quad (3)$$

i.e.,

$$\dot{\hat{i}}_b = -\frac{3R_s}{3L} i_b + \frac{1}{3L}(u_{bc} - u_{ab}) - \frac{2}{3L} e_b \quad (4)$$

Torque and motion equations are:

$$T_e = (e_a i_a + e_b i_b + e_c i_c) / \Omega \quad (5)$$

where,

- $T_e$  = Electromagnetic torque
- $\Omega$  = Mechanical angular velocity

### THE ESTABLISHMENT OF PHASE BACK-EMF OVSERVER

In (4),  $e_b$  could be regarded as a disturbance signal with regular change and  $\hat{i}_b$  could be estimated from (4). Since  $i_b$  is measurable in fact,  $\hat{i}_b$  could be used for comparison with  $i_b$  to obtain  $erro_{ib}$ , which could reflect the change of  $e_b$  and  $erro_{ib} = i_b - \hat{i}_b$ . Hence, the following formula could be obtained after introducing  $erro_{ib}$  in (6):

$$\dot{\hat{i}}_b = -\frac{R_s}{L} \hat{i}_b + \frac{1}{3L}(u_{bc} - u_{ab}) - \frac{2}{3L} e_b + k_4 erro_{ib} \quad (6)$$

where,  $k_4$  is gain coefficient.

In (6),  $erro_{ib}$  will be zero if  $\hat{i}_b$  is equal to  $i_b$  and then (6) will be same as (4), showing that estimated value and actual value of  $e_b$  are equal. If  $\hat{i}_b$  is not equal to  $i_b$ ,  $erro_{ib}$  will reflect the change of  $e_b$ . For establishing the relationship between  $erro_{ib}$ ,  $\hat{i}_b$  and  $\hat{e}_b$ , formula (7) is introduced (Changliang *et al.*, 2005; Shao, 2006):

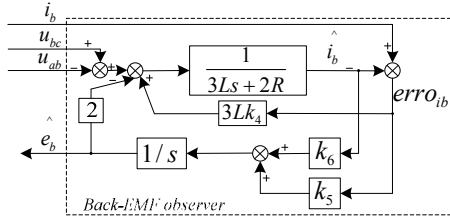


Fig. 1: The back-EMF observer of B phase

$$\dot{\hat{x}}_b = k_5 error_{ib} + k_6 \hat{i}_b \quad (7)$$

where,  $k_5$  and  $k_6$  are gain coefficient and an accurate  $e_b$  could be obtained through properly selecting  $k_5$  and  $k_6$ .

The back-EMF observer of phase B could be acquired as shown in Fig. 1.

Similarly, the observer models of the other two phases could be obtained and the system observer model could be obtained eventually:

$$\dot{\hat{x}} = A\hat{x} + Bu + K \times Error_i \quad (8)$$

where,

$$\hat{x} = \begin{bmatrix} \hat{i}_a \\ \hat{e}_a \\ \hat{i}_b \\ \hat{e}_b \\ \hat{i}_c \\ \hat{e}_c \end{bmatrix}; A = \begin{bmatrix} \frac{3R}{3L} & \frac{2}{3L} & 0 & 0 & 0 & 0 \\ k_3 & 0 & 0 & 0 & 0 & 0 \\ 0 & 0 & \frac{3R}{3L} & \frac{2}{3L} & 0 & 0 \\ 0 & 0 & k_6 & 0 & 0 & 0 \\ 0 & 0 & 0 & 0 & \frac{3R}{3L} & \frac{2}{3L} \\ 0 & 0 & 0 & 0 & k_9 & 0 \end{bmatrix}$$

$$B = \begin{bmatrix} 1/3L & 0 & 0 \\ 0 & 0 & 0 \\ 0 & 1/3L & 0 \\ 0 & 0 & 0 \\ 0 & 0 & 1/3L \\ 0 & 0 & 0 \end{bmatrix}; K = \begin{bmatrix} k_1 & 0 & 0 \\ k_2 & 0 & 0 \\ 0 & k_4 & 0 \\ 0 & k_5 & 0 \\ 0 & 0 & k_7 \\ 0 & 0 & k_8 \end{bmatrix}$$

$$u = \begin{bmatrix} u_{ab} - u_{bc} \\ u_{bc} - u_{ab} \\ u_{ca} - u_{ab} \end{bmatrix}; Error_i = \begin{bmatrix} error_{ia} \\ error_{ib} \\ error_{ic} \end{bmatrix} = \begin{bmatrix} i_a - \hat{i}_a \\ i_b - \hat{i}_b \\ i_c - \hat{i}_c \end{bmatrix}$$

Adjusting the structure of (9) and letting:

$$h_1(t) = (u_{ab}(t) - u_{bc}(t)) / [3L(i_a(t) - \hat{i}_a(t-1))] \quad (9)$$

$$h_4(t) = (u_{bc}(t) - u_{ca}(t)) / [3L(i_b(t) - \hat{i}_b(t-1))] \quad (10)$$

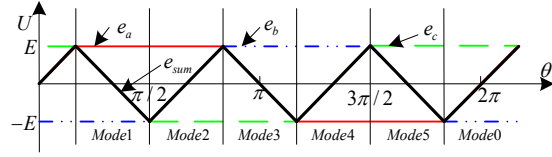


Fig. 2: Waveform of  $e_a$ ,  $e_b$ ,  $e_c$  and  $e_{sum}$

$$h_7(t) = (u_{ca}(t) - u_{ab}(t)) / [3L(i_c(t) - \hat{i}_c(t-1))] \quad (11)$$

The following formula could be obtained:

$$\dot{\hat{x}}(t) = A\hat{x}(t) + B'(t)u'(t) \quad (12)$$

The output formula is:

$$y(t) = C\hat{x}(t) \quad (13)$$

where,

$$B'(t) = \begin{bmatrix} h_1(t) - k_1 & 0 & 0 \\ k_2 & 0 & 0 \\ 0 & h_4(t) - k_4 & 0 \\ 0 & k_5 & 0 \\ 0 & 0 & h_7(t) - k_7 \\ 0 & 0 & k_8 \end{bmatrix}; C = \begin{bmatrix} 1 \\ 0 \\ 1 \\ 0 \\ 1 \\ 0 \end{bmatrix}^T$$

$$u'(t) = \begin{bmatrix} i_a(t) - \hat{i}_a(t-1) \\ i_b(t) - \hat{i}_b(t-1) \\ i_c(t) - \hat{i}_c(t-1) \end{bmatrix}; k_2, k_3, k_8 \neq 0; k_5, k_6, k_9 < 0$$

From (12) and (13), (14) and (15) can be concluded.

$$Rank([B' \ AB' \ A^2B' \ A^3B' \ A^4B' \ A^5B']) = 6 \quad (14)$$

$$Rank([C \ CA \ CA^2 \ CA^3 \ CA^4 \ CA^5]^T) = 6 \quad (15)$$

Hence, the system is completely controllable, completely observable and stability and the observer is fully feasible.

### HIGH-SPEED COMMUTATION METHOD

The back-EMF functions of BLDCM could be obtained according to its back-EMF's waveform shown in Fig. 2 and they are given in Table 1.  $e_{sum}$  could be obtained from Table 1 and  $e_{sum} = e_a + e_b + e_c$ .

The waveform of  $e_{sum}$  is shown in Fig. 2, which shows that the period of  $e_{sum}$  is one third of that of phase back-EMF. There are six zero-crossing points in each three periods and they are in accordance with six zero-

Table 1: The back-EMF function of BLDCM

$\theta_r$	$e_a$	$e_b$	$e_c$
0-30°	$(6E/\pi)\theta_r$	-E	E
30°-90°	E	-E	$-(6E/\pi)\theta_r+2E$
90°-150°	E	$-(6E/\pi)\theta_r+4E$	-E
150°-210°	$(6E/\pi)\theta_r+6E$	E	-E
210°-270°	-E	E	$-(6E/\pi)\theta_r+8E$
270°-330°	-E	$-(6E/\pi)\theta_r+10E$	E
330°-360°	$(6E/\pi)\theta_r+12E$	-E	E

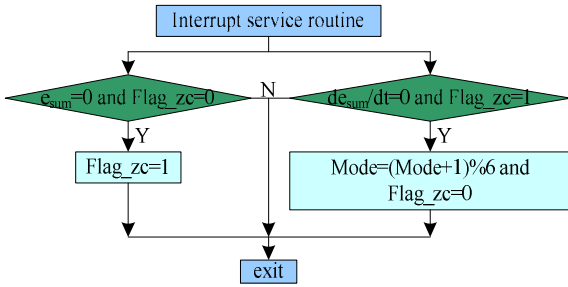


Fig. 3: Interrupt service routine of commutation point detection at high speed

crossing points of three-phase back-EMF in one period. In particular, the extreme point of  $e_{sum}$  is the commutation point of BLDCM.

At high speed, the commutation point could be determined through detection of the zero-crossing point and extreme point of  $e_{sum}$ . Figure 3 shows the interrupt service routine of commutation point detection and Mode = 1, 2, 3, 4, 5, 0 are corresponding to respective communication mode. But at low speed, the amplitude of  $e_{sum}$  is small and it is easy to cause unexpected commutation.

### LOW-SPEED COMMUTATION METHOD

In order to solve the low-speed commutation problem of BLDCM, a novel commutation function for determining commutation points is provided in this study. The function can realize low-speed control of BLDCM perfectly.

The commutation functions are:

$$CF(\theta)_1 = \hat{e}_a / (\hat{e}_b - \hat{e}_c) \quad (16)$$

$$CF(\theta)_2 = \hat{e}_b / (\hat{e}_c - \hat{e}_a) \quad (17)$$

$$CF(\theta)_3 = \hat{e}_c / (\hat{e}_a - \hat{e}_b) \quad (18)$$

The working principle of the commutation function is shown in Fig. 4. In Fig. 4a,  $CF_1$  is negative when  $\theta$  is in  $0 \sim \pi/2$  and  $CF_1$  decreases gradually.  $CF_1$  decreases rapidly towards negative infinity when  $\hat{e}_b - \hat{e}_c$  approaches zero. Just after  $\theta$  entering  $\pi/2 \sim \pi$ ,  $CF_1$  turns from negative infinity to positive infinity immediately and

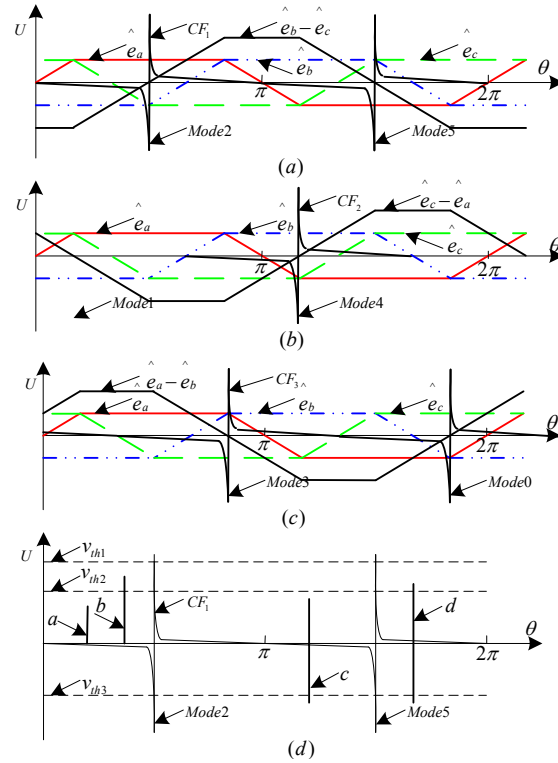


Fig. 4: Working principle of the commutation functions

this moment corresponds to the commutation moment of Mode2.  $CF_1$  decreases quickly with increasing of  $\theta$ , but  $CF_1$  is positive during this section.  $\hat{e}_a$  becomes negative after  $\theta$  entering  $\pi \sim 3\pi/2$ , but  $\hat{e}_b - \hat{e}_c$  remains positive and  $CF_1$  becomes negative with small absolute value.  $CF_1$  approaches negative infinity immediately when  $\theta$  approaches  $3\pi/2$ . After  $\theta$  entering  $3\pi/2 \sim 2\pi$  section,  $CF_1$  becomes positive infinity quickly, for  $\hat{e}_b - \hat{e}_c$  turns from positive to negative and the moment corresponds to the commutation moment of Mode 5. With continuous increasing of  $\theta$ ,  $CF_1$  decreases quickly and it remains positive with small absolute value in this section. Similarly, the commutation points of Mode 1 and Mode 4 could be obtained from  $CF_2$  (Fig. 4b) and the commutation points of Mode 3 and Mode 0 could be obtained from  $CF_3$  (Fig. 4c). Because the range of data processed by microprocessor is limited, commutation points could be detected through setting proper threshold values.

Figure 4d shows  $CF_1$  under disturbance signal. Because the amplitude of noise  $a$  is smaller than  $v_{th2}$ , it could be filtered. The amplitude of the noise  $b$  exceeds  $v_{th2}$ , but it does not turns from negative to positive immediately, so it could also be filtered. The negative maximum value of noise  $c$  exceeds  $v_{th3}$ , but the positive maximum value of it does not exceeds  $v_{th2}$ , so it could also be filtered. The negative maximum value of the noise  $d$  exceeds  $v_{th3}$  and the positive maximum value exceeds  $v_{th2}$ , so the noise  $d$  is regarded as a commutation

Table 2: The expression of  $e_{sum}$  in a whole period

$\theta_r$	$e_{sum}$	$\theta_r$	$e_{sum}$
0-30°	$(6E/\pi)\theta_r$	90°-120	$(6E/\pi)\theta_r-4E$
30°-90°	$-(6E/\pi)\theta_r+2E$		

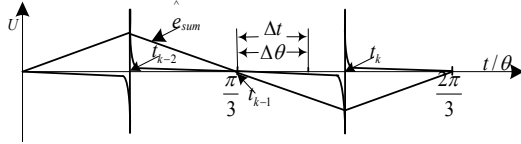


Fig. 5: Relationship between commutation points and  $\hat{e}_{sum}$

point. This phenomenon could be filtered through adjusting the threshold value according to work environment, such as increasing  $v_{th2}$  to  $v_{th1}$  or combining with other filter methods.

### ROTOR SPEED AND TORQUE CONTROL AND POSITION TRACKING

At high speed, rotor speed and position could be determined through detecting  $\hat{e}_{sum}$ , as shown in Table 2. At low speed, for the amplitude of back-EMF is small,  $\hat{\omega}_r$  and  $\hat{\theta}$  could be obtained through determining the time interval between the commutation point and the sign changing point of  $\hat{e}_{sum}$  and the displacement between them is  $\pi/6$ . The position relationship between the commutation point and  $\hat{e}_{sum}$  is shown in Fig. 5 and the calculation method is given as followed:

$$\omega_{r,k-1} = \frac{6/\pi}{t_{k-1} - t_{k-2}}; \omega_{r,k} = \frac{6/\pi}{t_k - t_{k-1}} \quad (19)$$

$$\Delta\theta = \frac{\Delta t}{t_{k-1} - t_{k-2}} \times \frac{\pi}{6} \quad (20)$$

where,

$\omega_{r,k}$  = the angular velocity of motor at moment  $t_k$

$\Delta\theta$  = the angular displacement in  $\Delta t$

The equation of estimated speed is:

$$\hat{\Omega} = \frac{2}{P_n} \hat{\omega}_r; \hat{n} = \frac{60}{2\pi} \hat{\Omega} \quad (21)$$

And the estimating equation of torque is:

$$\hat{T}_e = (\hat{e}_a \hat{i}_a + \hat{e}_b \hat{i}_b + \hat{e}_c \hat{i}_c) / \hat{\Omega} \quad (22)$$

### SIMULATION AND EXPERIMENTAL RESULTS ANALYSIS

The control block diagram of BLDCM is shown in Fig. 6 and parameters of BLDCM are given in Table 3.

Table 3: Parameter table of BLDC motor

Rated voltage	V	310V	Stator inductance	L	5.22 mH
Rated torque	$T_e$	12Nm	Rotor inertia	J	0.08 kg·m <sup>2</sup>
Rated speed	n	1000	Number of pole pairs	$P_n$	2
Stator resistance	$R_s$	1.5Ω			

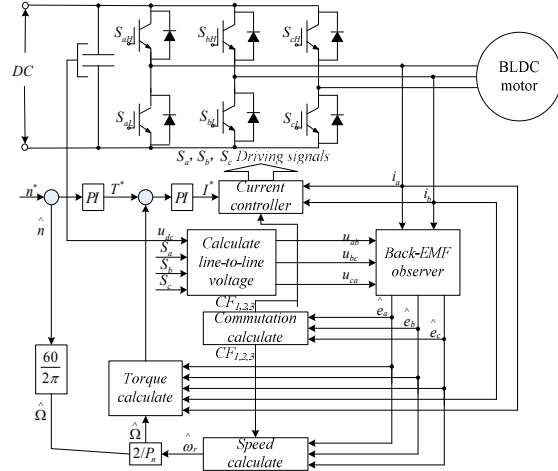
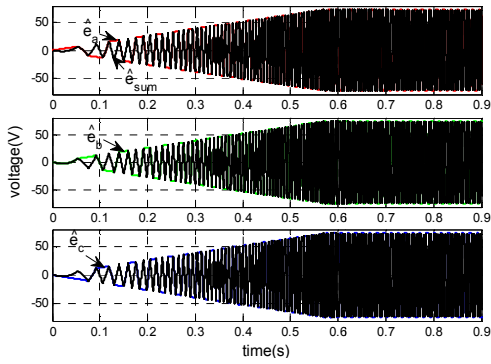


Fig. 6: The block diagram of control system

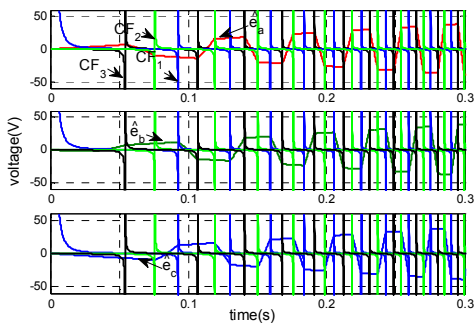
The Matlab/Simulink platform is used for system simulation, which includes three conditions ( $\max(dn/dt) = 2000$  rpm):

- If the given speed is 1000 rpm and a torque of 12Nm is suddenly added at 0.7s, simulation results are shown in Fig. 7.
- If the given speed is 30 rpm and a torque of 12Nm is suddenly added at 0.3s, simulation results are shown in Fig. 8.

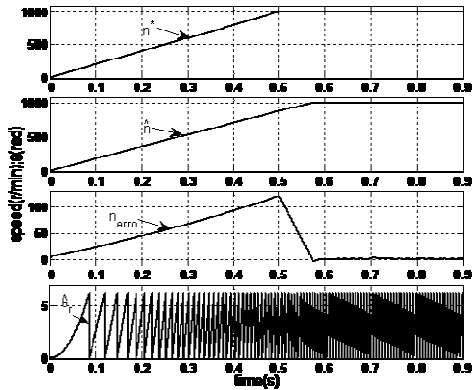
In Fig. 7a and 8a, the period of  $\hat{e}_{sum}$  is 1/3 of that of phase back-EMF and zero-crossing points of  $\hat{e}_{sum}$  in each three cycles are the same as those of three-phase phase back-EMFs in one cycle. Figure 7b and 8b show that changing points of  $CF_{1,2,3}$  from the negative infinity to the positive infinity are corresponding to commutation points at low speed, hence the problem of determining commutation moment at low speed could be properly solved. Figure 7c and 8c show the results of speed control and position tracking. Figure 7c shows that the actual speed is slower than the given speed before 0.6 second at high speed.  $n_{error}$  reaches its maximum 0.1s before entering the steady state and then decreases quickly with a little overshoot. At low speed, since the given speed is relatively small, speed enters into steady state within 0.05s and the maximum speed error reaches 6 rpm in Fig. 8c. When the torque is suddenly added, the speed reduces nearly 3 rpm immediately and then enters into steady state as shown in Fig. 7c and 8c. Figure 7d and 8d show the system response for torque and it can be seen that the output torque could follow the change of reference torque.



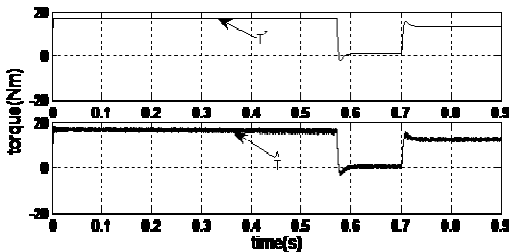
(a) Waveforms of  $\hat{e}_a$ ,  $\hat{e}_b$ ,  $\hat{e}_c$  and  $\hat{e}_{sum}$



(b) Waveforms of  $\hat{e}_a$ ,  $\hat{e}_b$ ,  $\hat{e}_c$ ,  $CF_1$ ,  $CF_2$  and  $CF_3$  at low speed

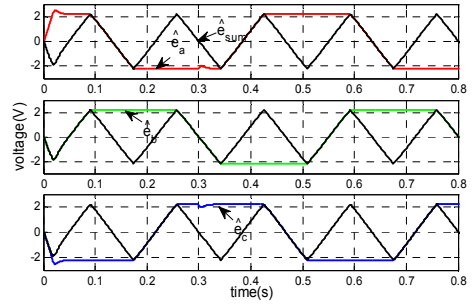


(c) The curves of given speed, estimated actual speed, speed error and estimated rotor position

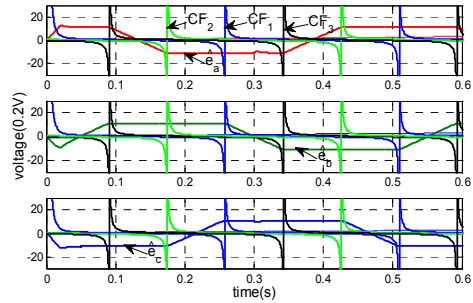


(d) The given torque curve and the estimated torque curve

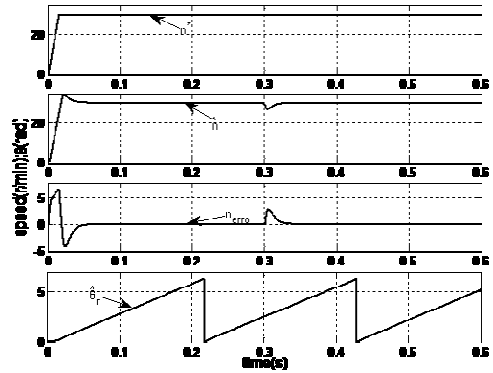
Fig. 7: The simulation results after adding a 12Nm torque at 0.7s



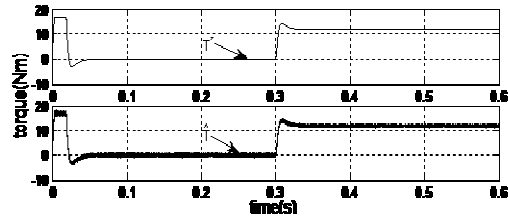
(a) Waveforms of  $\hat{e}_a$ ,  $\hat{e}_b$ ,  $\hat{e}_c$  and  $\hat{e}_{sum}$



(b) Waveforms of  $\hat{e}_a$ ,  $\hat{e}_b$ ,  $\hat{e}_c$ ,  $CF_1$ ,  $CF_2$  and  $CF_3$  at low speed



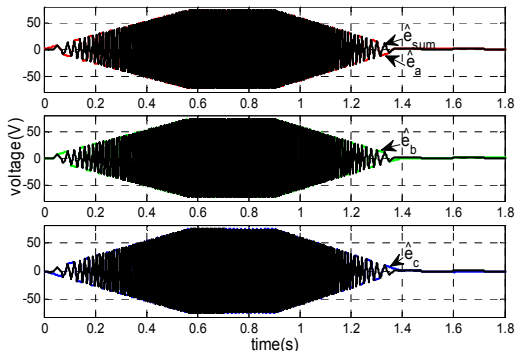
(c) The curves of given speed, estimated actual speed, speed error and estimated rotor position



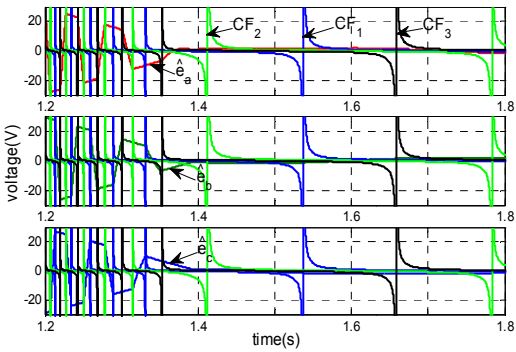
(d) The given torque curve and the estimated torque curve

Fig. 8: Simulation results after suddenly adding a 12Nm torque at 0.3s under the given speed of 30 rpm

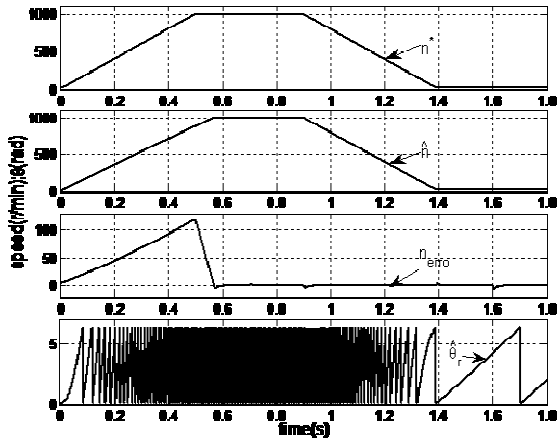
- If the initial given speed is 1000 rpm and a load torque of 12Nm is suddenly added at 0.7s, given speed is changed to be 20 rpm at 0.9s and a load torque of -12Nm is suddenly added at 1.6s, the simulation results are shown in Fig. 9.



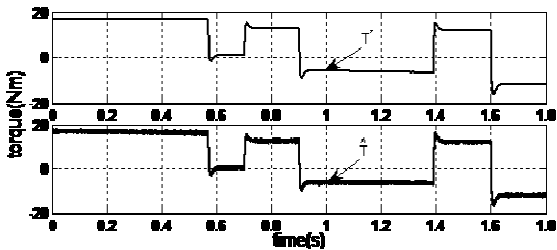
(a) Waveforms of  $\hat{e}_a$ ,  $\hat{e}_b$ ,  $\hat{e}_c$  and  $\hat{e}_{sum}$



(b): Waveforms of  $\hat{e}_a$ ,  $\hat{e}_b$ ,  $\hat{e}_c$ ,  $CF_1$ ,  $CF_2$  and  $CF_3$  at low speed



(c) The curves of given speed, estimated actual speed, speed error and estimated rotor position



(d) The given torque curve and the estimated torque curve

Fig. 9: Simulation results of case 3

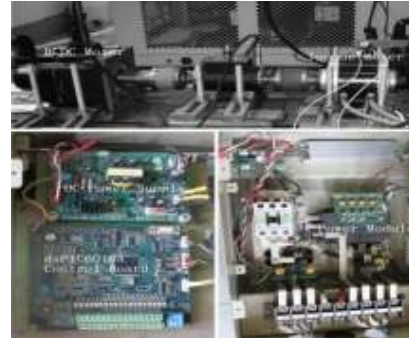
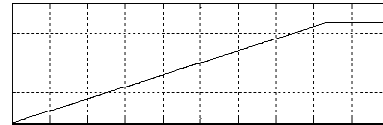
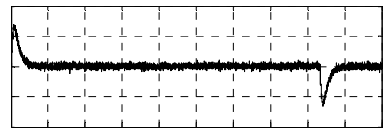


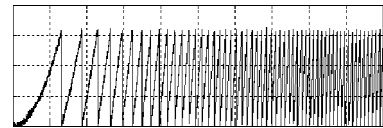
Fig. 10: The overall experimental test-system



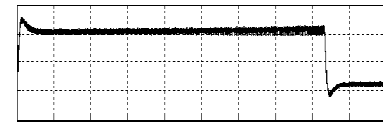
(a)  $\hat{n}$  (Y-axis:300 rpm/div, X-axis:100ms/div)



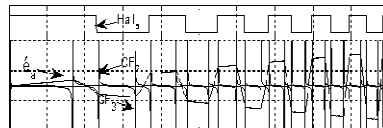
(b)  $n_{err}$  (Y-axis:5 rpm/div, X-axis:100ms/div)



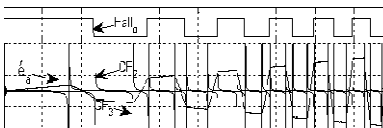
(c)  $\hat{\theta}$  (Y-axis:2rad/div, X-axis:100ms/div)



(d)  $\hat{T}$  (Y-axis:10Nm/div, X-axis:100ms/div)



(e)  $\hat{e}_s$ ,  $\hat{e}_{sum}$  (Y-axis:80V/div, X-axis:100ms/div)

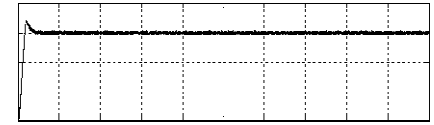


(f)  $Hall_a$  (Y-axis:10V/div, X-axis:30ms/div),  $\hat{e}_a$  (Y-axis:20V/div, X-axis:30ms/div)

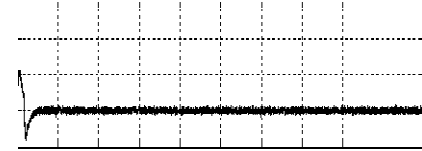
Fig. 11: Waveforms under load torque of 2Nm and given speed of 1000 rpm

In Fig. 9a, the period of  $\hat{e}_{sum}$  is 1/3 of that of phase back-EMFs at both high speed and low speed and zero points of  $\hat{e}_{sum}$  in each three cycles are the same as those of the three-phase phase back-EMFs in one cycle. The figure also shows that the observer detects the phase back-EMF effectively. In Fig. 9b, changing points of  $CF_{1,2,3}$  from the negative infinity to the positive infinity are corresponding to commutation points at low speed, which properly solves the problem of determining the commutation moment at low speed. The Fig. 9c shows the results of speed control and position tracking. It is shown that the actual speed is slower than the given speed before 0.6 second in start-up process and  $n_{error}$  reaches its maximum at 0.5s. Then the error decreases quickly with little overshoot and speed enters into steady state later. When the load torque is suddenly added at 0.7s, the speed reduces slightly and enters into steady state without error after transient adjustment. The given speed is suddenly reduced at 0.9s and the speed deviation is generated instantaneously. The speed keeps up with the given speed after an adjustment for 0.1s and reaches the given speed of 20 rpm at 1.5s after a little overshoot. The minus torque is suddenly added at 1.6s and the speed reduces immediately. It enters into steady state without error after an adjustment for 0.1s. 9(d) shows the system response for the torque and it can be seen that the output torque could follow the change of reference torque perfectly.

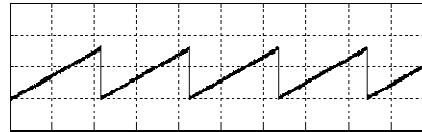
The system experimental platform using dsPIC6010A as CPU is established based on the above-mentioned method and is shown in Fig. 10. The system working principle is shown in Fig. 6 ( $max (dn/dt) = 2000$  rpm). Motor parameters are given in Table 3 and experimental results are shown in Fig. 11 and 12. Figure 11 and 12 show estimated speed, speed error, estimated position, estimated output torque, estimated waveforms for  $\hat{e}_a$  and  $\hat{e}_{sum}$ , waveform comparison of  $Hall_a$ ,  $\hat{e}_a$ ,  $CF_1$  and  $CF_2$  under the given load torque of 2Nm and given speed of 1000 rpm and 30 rpm respectively. Figure 12f shows that if the given speed is high, there is an electrical angle lag of  $6^\circ \sim 7^\circ$  between commutation point estimation signal and Hall signal in start-up process. With the fast increasing of the speed, the lag decreases and the lag is almost disappeared at 0.28s. In Fig. 12(f), for the given speed is slow, the system enters into steady state in less than 0.1s. Just after it enters into steady state, there is an electrical angle lag of about  $2^\circ$  between corresponding commutation point estimation signal and Hall signal. But later they are almost synchronous. The reason of lag is that the speed changes quickly and there is first-order inertia link and integrator in back-EMF observer. This lag also causes the pulsation of torque and the lag of speed response and further affects estimated accuracy of rotor position. However, in general the proposed control method shows good dynamic responses over whole speed range operation.



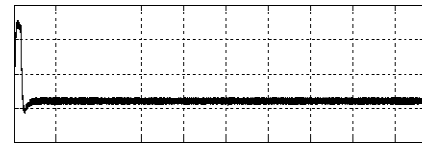
(a)  $\hat{n}$  (Y-axis:10 rpm/div, X-axis:100ms/div)



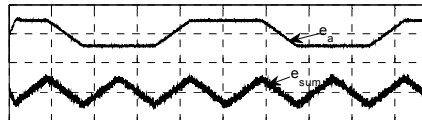
(b)  $n_{error}$ (Y-axis:5 rpm/div, X-axis:100ms/div)



(c)  $\hat{\theta}_r$  (Y-axis: 3rad/ div, X-axis:100ms/div)



(d)  $\hat{T}$  (Y-axis:10Nm/div, X-axis:100ms/div)



(e)  $\hat{e}_a, \hat{e}_{sum}$  (5V/div,100ms/div)



(f)  $Hall_a$  (10V/div, 100ms/div),  $\hat{e}_a$  (5V/div, 100ms/div)

Fig. 12: Waveforms under the load torque of 2Nm and given speed of 30 rpm

The maximum changing rate ( $max (dn/dt) = 2000$  rpm) of speed is limited for hardware consideration and the phase lag is relatively large shortly after start up. Compared with (Furuhashi *et al.*, 1990), the system has only one inertia link, hence, its transition process is significantly faster and there is not any static error for steady state at both low speed range and high speed range, which show the effectiveness of the method.

### CONCLUSION

A novel detection method for the phase back-EMF of BLDCM is proposed in this study and this algorithm

carries out the estimation through regarding phase back-EMF as disturbance signal. Simulation and experimental results show that this algorithm could effectively estimate the phase back-EMF and carry out commutation precisely. Advantages of this algorithm are: additional detection circuits could be avoided; precise commutation could be carried out both in steady state and transient state; the motor speed could be precisely controlled in full range; the position tracking and torque control of the BLDCM could be achieved, especially in large rated torque motor.

#### ACKNOWLEDGMENT

This study was supported by Science and technology pillar Key Program of Tianjin (11ZCZDSF04800) and Universities Science and Technology Fund Planning Project of Tianjin (20100713).

#### REFERENCES

- Bharatkar, S.S. and R. Yanamshetti, 2010. Comparison of switching schemes for brushless DC Motor Drives. ECTI-CON 2010, Chaing Mai, pp: 1036-1040.
- Changliang, X., J. Liu, W. Yu and Z. Li, 2005. Variable structure control of BLDCM based on extended state observer. International Conference on Mechatronics and Automation, Chengdu, Sichuan, China, pp: 568-571.
- Changliang, X., L. Junhua, Y. Wei and Z. Li, 2006. Variable structure control of BLDCM based on extended state observer. Proceedings of the CSEE, 26(20): 139-153.
- Furuhashi, T., S. Sangwongwanich and S. Okuma, 1990. A position and velocity sensorless control of brushless DC motors using an adaptive sliding observer. Proceeding of IEEE IECON'90, Pacific Grove, CA, pp: 1188-1192.
- Guan, E., S. Pinggang and Y. Xiaoyu, 2005. BLDC Motor based on the detecting method of fow-wheeling diodes. Explosion-Proof Electric Mach., 40(1): 24-28.
- Kim, J.S. and S.K. Sul, 1995. High performance PMSM drives without rotational position sensors using reduced order observer. Proceeding of Conference on IEEE IAS Annu. Meeting, Orlando, FL, pp: 75-82.
- Shao, J., 2006. An improved microcontroller based sensorless brushless DC (BLDC) motor drive r for automotive applications. IEEE T. Indus. Appl., 52(5): 1216-1221.
- Tae-Sung, K., 2008. A new approach to sensorless control method for brushless DC motors. Int. J. Contr. Autom. Syst., 6(5): 577-587.
- Ungurean, A., V. Coroban-Schramel and I. Boldea, 2010. Sensorless control of a BLDC PM motor based on I-f starting and Back-EMF zero-crossing detection. OPTIM 2010, Basov, pp: 377-382.
- Wang, H. and H. Liu, 2008. Novel driving method for BLDCM from standstill to high speeds. Wseas T. Syst., 11(7): 1269-1279.
- Wang, K., M.A. Rahman and J.X. Shen, 2010. control of high-speed sensorless PM brushless DC motors. Industry Applications Society Annual Meeting (IAS), 2010 IEEE, Houston, TX USA, pp: 1-7.
- Xianxiang, L., Z. Zifang and Z. Huimin, 2009. A position sensorless motion control system of brushless DC Motor motor based on sliding mode observer [J]. J. Circuits Syst., 15(2): 79-83.
- Yen-Shin, L., 2004. Novel initial position detection technique for three-phase brushless DC motor without position and current sensors. 39th IAS Annual Meeting, Seattle, WA, USA, pp: 2377-2381.
- Zicheng, L., C. Shanmei and C. Kai, 2009. A novel scheme of sensing rotor position of BLDCM based on the zero-crossing of back EMF. T. China Electrotechnical Soc., 24(7): 52-58.